Nanoscale Advances

ROYAL SOCIETY OF CHEMISTRY

PAPER

View Article Online
View Journal

Cite this: DOI: 10.1039/d5na01139f

Fluorescent nanocellulose derived from *Plectranthus barbatus* for the selective detection of Pb(II) ions in aqueous solutions

Joshua Jose,*[a] Aishwarya Joji Mathew,[a] Elizabeth Gabriel,[a] Ancilin James[a] and T. P. Vinod *[ab]

This study reports the synthesis of fluorescent nanocellulose from *Plectranthus barbatus* and its effective use as a fluorescent probe for the detection of Pb(II) ions in aqueous solutions. Nanocellulose, a nanoscale derivative of cellulose, is used in a variety of applications, such as sensing, food packaging, and biomedical applications, owing to its characteristic properties. In sensing applications, it is mostly used as a support or substrate for the sensing probe. Nanocellulose shows intrinsic fluorescence, which can be harnessed for sensing applications. This underexplored research domain holds significant potential for developing sustainable and cost-effective sensing materials. We synthesized nanocellulose from *Plectranthus barbatus* (PBNC) and employed it as a fluorescent probe for the detection of Pb(II). To the best of our knowledge, this is the first report demonstrating the potential of fluorescent nanocellulose for metal ion detection. The properties of fluorescent nanocellulose, PBNC, were studied using Fourier Transform Infrared (FTIR) spectroscopy, X-ray Diffraction (XRD), Transmission Electron Microscopy (TEM), and Photoluminescence (PL) spectroscopy. The fluorescence intensity of the nanocellulose was remarkably quenched in the presence of Pb(II) ions selectively. The detection limit (LOD) of Pb(II) using PBNC was found to be 2.7 nM. PBNC is a novel autofluorescent material that functions as an efficient nanosensor for the detection of Pb(II) ions, and its applications can be extended to bio-imaging and sensing in biological, chemical, and environmental samples.

Received 17th December 2025
Accepted 20th April 2026

DOI: 10.1039/d5na01139f

rsc.li/nanoscale-advances

1 Introduction

Cellulose, a plant-based polysaccharide, is composed of polymerized β-D-glucopyranose units that form a distinctive structural framework.[1] Miniaturization of cellulose results in the formation of nanocellulose or cellulose nanomaterials, which exhibit enhanced structural, mechanical, and optical properties, thereby broadening their spectrum of applications.[2] Nanocellulose is widely used in biosensors and chemical sensors owing to the abundance of functional groups, high surface area, and flexibility.[3] In most of its applications in sensors, nanocellulose is used as a substrate to host the probe material.[4] Nanocellulose is not considered an active sensor component, as it generally lacks the optical and electrochemical properties required to generate and acquire analytical responses.[5] Contrary to the common perception of nanocellulose as an inert material with respect to signal generation, recent findings reveal that it exhibits intrinsic autofluorescence, thereby unlocking new potential for sensor applications. Autofluorescence in nanocellulose is an inherent property, without any fluorescent labels or impurities being added to it.[6] The cause of autofluorescence in nanocellulose is still obscure, as there are no aromatic groups or π-conjugation in its structure, which is considered to be a prerequisite for photoluminescence in organic compounds.[7] The most prominent theory regarding autofluorescence in nanocellulose is clustering-triggered emission (CTE).[8] According to this theory, the electron-rich functional groups (carbonyls, hydroxyls, *etc.*) in nanocellulose interact through space, thereby reducing the band gap of nanocellulose, resulting in emissions.[9] In nanocellulose, the abundant oxygen-rich groups, along with the presence of hydrogen bonds, are considered to manifest the fluorescence.[10] Autofluorescence of nanocellulose remains an underexplored phenomenon, which offers significant and untapped potential for sensing applications. They have the potential to be used efficiently and effectively in heavy metal ion detection, environmental monitoring, biomedical engineering and food safety analysis.[11]

Plectranthus barbatus was selected as the precursor for the synthesis of nanocellulose owing to its high content of polyphenols and flavonoids, which can function as intrinsic fluorophores or fluorescence-enhancing agents upon conversion to nanocellulose.[12] This inherent phytochemical richness supports the development of environmentally benign, green

[a]*Department of Chemistry, Christ University, Hosur Road, Bengaluru 560029, India*
[b]*Centre for Renewable Energy and Environmental Sustainability, Christ University, Bengaluru 560029, India. E-mail: vinod.tp@christuniversity.in*

fluorescent sensing platforms. Furthermore, the abundance of oxygen-containing functional groups provides effective coordination sites for Pb(II) ions, contributing to enhanced selectivity toward Pb(II).[13] In addition, *Plectranthus barbatus* is inexpensive, renewable, and widely available, rendering it a sustainable lignocellulosic feedstock for scalable nanocellulose production.[14]

In the present study, we synthesized a novel autofluorescent nanocellulose from the *Plectranthus barbatus* plant through optimised pretreatment and acid hydrolysis procedures. The autofluorescent *Plectranthus barbatus* nanocellulose (PBNC) was used as a fluorescent probe for the detection of Pb(II) ions in aqueous solutions. The nanocellulose showed good selectivity towards Pb(II) ions with a detection limit of 2.7 nM. To the best of our knowledge, this work represents the first report on the application of autofluorescent nanocellulose for the detection of Pb(II) ions. The sensitivity, selectivity, and simplicity of this sensor system are comparable to those of other nanocellulose-based systems, offering a novel and effective strategy for the fluorescent detection of a highly toxic heavy metal.

2 Materials and methods

2.1 Chemicals

The *Plectranthus barbatus plant* was collected from Begur village, Bengaluru, India. Sodium hydroxide (NaOH), hydrogen peroxide (H_2O_2), sulphuric acid (H_2SO_4), qunine sulphate (QS), $MnSO_4$, $BaCl_2$, $NiSO_4$, $HgCl_2$, $AlCl_3$, $FeCl_2$, NaCl, $PbCl_2$, $Na_2HPO_4{\cdot}12H_2O$, and NaH_2PO_4, were purchased from Sigma-Aldrich. Syringe filters (Nylon, pore size 0.22 μm) and Dialysis membrane-70 (flat width −28.46 mm, diameter −17.5 mm, and molecular weight cut-off of 1200 Da to 1400 Da) were procured from HiMedia Laboratories, India.

2.2 Synthesis of *Plectranthus barbatus* nanocellulose (PBNC)

2.2.1 Pretreatment of the *Plectranthus barbatus* plant. The *Plectranthus barbatus* plant was subjected to alkali treatment and bleaching in order to remove the lignin and hemicellulose content, using previously reported procedures.[15,16] The *Plectranthus barbatus* plant was first cleaned and thoroughly washed with water and then dried in sunlight for two days. Then it was ground into powder form and dried. 5 g of the powder was weighed and added to 100 ml of 5% (w/v) NaOH solution. The mixture was then stirred for one hour at 75 °C. The resultant reaction mixture was washed with water until a neutral pH was reached and then dried. This step is crucial in the delignification process of the fiber, as it determines the quality and color of the resulting cellulose. The delignified sample was added to 100 ml of a solution containing 4% NaOH (w/w) and 24% hydrogen peroxide (v/v) in a 1 : 1 ratio, and the mixture was stirred vigorously for two hours. The resulting residue was then washed with water and sun dried to obtain the *Plectranthus barbatus* cellulose.

2.2.2 Preparation of *Plectranthus barbatus* nanocellulose (PBNC). PBNC was prepared by the acid hydrolysis of *Plectranthus barbatus* cellulose, using previously reported procedures.[15,17]

5 g of *Plectranthus barbatus* cellulose was added to 100 ml of 35% (w/w) sulfuric acid. The mixture was then subjected to magnetic stirring for three hours at room temperature. Distilled water was added to the solution to stop the reaction. Following this, it was centrifuged for three cycles at 8500 rpm, with each cycle lasting 20 minutes. Following centrifugation, the acidic supernatant was removed and replaced with distilled water. The nanocellulose suspension was syringe filtered to remove residual matter. The resultant solution was then subjected to dialysis for 24 hours to remove acid residues. The nanocellulose collected from the membrane was vigorously stirred for 10 minutes to break down the particles. The resultant PBNC was then collected, refrigerated and used for characterization.

2.3 Characterization

Fourier transform infrared (FTIR) spectra with a frequency range of 4000 to 500 cm^{-1} and a spectral resolution of 4 cm^{-1} were obtained from the samples using a PerkinElmer Spectrum 100 spectrometer. A Bruker D Advance X-ray diffractometer (XRD) was used to perform the X-ray diffraction investigation using Cu Kα radiation with a wavelength of 1.5406 Å. The operating conditions of the diffractometer were set at 40 kV and 20 mA, and data were collected over a range of 10 to 90°. Scanning electron microscopy (SEM) images were obtained utilizing a Thermo Fisher Scientific Apreo 2S, with a maximum accelerating voltage of 30 kV. High-resolution transmission electron microscopy (HRTEM) images were acquired using a JEOL JEM-2100 LaB6, operating at 200 kV. The suspension's zeta potential was measured by dynamic light scattering (DLS) with a Zetasizer (ZS90) instrument. The optical properties of the nanocellulose were recorded using a UV-vis spectrophotometer (Shimadzu UV-1500) and fluorophotometer (Shimadzu RF-6000). PL lifetime measurements were recorded using a JOBIN-VYON M/S Fluorocube system.

2.4 Quantum yield (φ) calculation

The quantum yield of PBNC was calculated by the reference method using quinine sulphate ($\varphi = 54\%$) in 0.1 M H_2SO_4 as the reference. [18] The absorbance of aqueous solutions of PBNC and quinine sulphate was measured by keeping the optical density below 0.1 at a wavelength of 220 nm. Afterwards, the fluorescence intensities of the reference and PBNC were determined. The quantum yield for PBNC was calculated using the following equation.

$$\varphi_s = \varphi_R \left(\frac{I_S}{I_R}\right) \times \left(\frac{A_R}{A_S}\right) \times \left(\frac{{\eta_S}^2}{{\eta_R}^2}\right)$$

where, φ_S is the quantum yield of the sample, φ_R is the quantum yield of the reference, I_S is the fluorescence intensity of the sample, I_R is the fluorescence intensity of the reference, A_R is the optical density of the sample, A_S is the optical density of the reference, η_S is the refractive index of the sample, and η_R is the refractive index of the reference.

2.5 Detection of Pb(II) ions

For the detection of Pb(II) ions, 20 μL of the aqueous dispersion of PBNC was added to 3 ml of phosphate buffer solution of pH 7, followed by the serial addition (0–12 μl) of $PbCl_2$ of 10^{-5} M concentration. The PL spectra were recorded after incubation at room temperature for 5 minutes.

2.6 Evaluation of selectivity for Pb(II) in the presence of interfering ions

The selectivity of PBNC toward Pb(II) ions was investigated in the presence of potentially interfering metal ions. Briefly, 3 ml of buffer solution was mixed with 20 μL of PBNC dispersion, followed by the simultaneous addition of 20 μL aqueous solutions of individual metal ion (Pb(II), Al(III), Ba(II), Fe(II), Hg(II), Mn(II), Na(I), and Ni(II)) solutions of 10^{-5} M concentration. A solution prepared without Pb(II) was used as the control. In a separate set of experiments, 3 ml of buffer solution containing 20 μL of PBNC and 20 μL of Pb(II) was prepared, after which 20 μL of each interfering metal ion solution (Al(III), Ba(II), Fe(II), Hg(II), Mn(II), Na(I), and Ni(II)) was added individually to evaluate possible interference effects. After incubation at room temperature for 5 min, the photoluminescence (PL) spectra were recorded.

2.7 Analysis of real samples

The practical applicability of PBNC was tested through selective and sensitive detection of Pb(II) ions in lake water samples collected from Begur lake, Bangalore, India. The samples were pre-filtered using a 0.22 μm membrane to remove suspended particulates. Briefly, 3 ml aliquots of the filtered lake water were spiked with 20 μL of Pb(II) solutions at varying concentrations (10, 20, 30, 40, and 50 μM). Subsequently, 20 μL of PBNC was added to each analyte solution, and the fluorescence response was recorded upon excitation at 220 nm.

3 Results and discussion

We report the synthesis of fluorescent nanocellulose, PBNC, from the *Plectranthus barbatus* plant for the first time. Fluorescent PBNC was synthesised from *Plectranthus barbatus via* sequential mechanical processing, alkali delignification, bleaching, and H_2SO_4 hydrolysis, followed by dialysis and syringe filtration. The resultant fluorescent PBNC was utilized for the selective detection of Pb(II) ions in aqueous solutions (Fig. 1).

3.1 Structural characterisation at different stages of PBNC synthesis

The XRD and FTIR analyses at the different stages of synthesis of *Plectranthus barbatus* nanocellulose were used to confirm the removal of lignin and hemicellulose and the enhancement in crystallinity.[19] XRD analysis was carried out in order to analyse the increase in crystalline character during different synthesis stages of PBNC.[20] XRD patterns of PBNC exhibited three distinct peaks near 2θ values of 16°, 22°, and 34° corresponding to the (110), (002), and (004) planes of cellulose (Fig. S1, SI), which are characteristic crystalline peaks of cellulose.[21] During the synthetic procedure, the raw *Plectranthus barbatus* plant underwent successive chemical treatments to transform into delignified and then to bleached forms. Each stage of treatment showed a significant increase in crystallinity, as evident from Fig. S1, SI. This change in crystallinity is due to the chemical treatments that effectively removed amorphous components such as hemicellulose and lignin.[22] The comparison of the XRD peaks at different synthesis steps of PBNC reveals that the delignification and bleaching reactions did not alter the

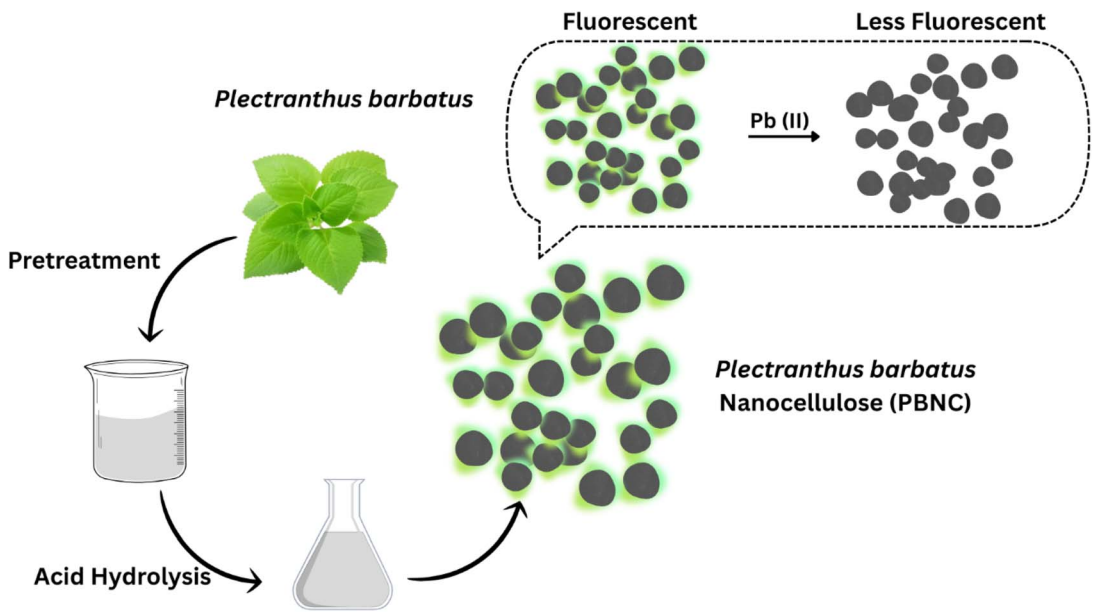

Fig. 1 Schematic representation for the preparation of PBNC for the selective detection of Pb(II) ions (created with Canva.com).

structure of cellulose, but removed the amorphous content. The observed increase in crystallinity is a relative effect due to the removal of amorphous lignin and partial removal of hemicellulose.[23]

The FTIR analysis was carried out to identify and characterize the functional groups in cellulose and nanocellulose.[24] Comparison of the FTIR spectra (Fig. S2, SI) of raw *Plectranthus barbatus*, delignified fiber, and bleached fiber shows a clear increment in the cellulose content in bleached fiber in comparison with the other two stages. The spectra of the raw and delignified *Plectranthus barbatus* fiber were found to be almost similar. Similar peaks of raw and delignified stages suggest that the sodium hydroxide delignification process did not induce any significant chemical and structural changes.[25] A significant peak was found in the FTIR spectrum at 1490.27 cm^{-1} in both raw and delignified stages, which indicates the presence of the $-CH_2$ deformation vibration in side chains.[26] This peak is characteristic of lignin, and it is absent in the spectrum of the bleached state, suggesting the removal of lignin. The peaks at 1644.44 cm^{-1} and 1518.82 cm^{-1} correspond to the stretching vibrations of C=O and the aromatic skeletal vibration of C=C in lignin, respectively.[27] These peaks were also absent in the spectra of the bleached sample, indicating that the bleaching procedure using hydrogen peroxide and sodium hydroxide could successfully remove lignin.[28] However, a characteristic peak at 1587.34 cm^{-1} with notable intensity remained in the bleached samples, suggesting that the bleaching process did not fully eliminate the hemicellulose from the sample.[29] Additionally, peaks were observed in the spectra of the raw, delignified, and bleached samples at 3340.81 cm^{-1} for the –OH stretching vibration, at 2894.91 cm^{-1} for the C–H stretching vibration, at 1421.76 cm^{-1} for $-CH_2$ and –OCH– plane bending vibrations, at 1381.79 cm^{-1} for the C–H deformation vibration, and at 907.87 cm^{-1} for the anomeric carbon (C1) vibration.[30] These are all distinctive peaks of cellulose, demonstrating that highly pure cellulose was obtained. It is very much evident from the FTIR analysis that the characteristic peaks of bleached samples coincide with the reported FTIR peaks of cellulose, thus confirming the synthesis of pure cellulose from *Plectranthus barbatus*.

3.2 Structural characterization of PBNC

HRTEM analysis was carried out to understand the structural and morphological characteristics of the nanocellulose.[31] The TEM images (Fig. 2a) revealed the quasi-spherical morphology of the synthesised PBNC. The histogram (Fig. 2b) depicting the size distribution of PBNC shows that the average size is around 38 nm. The lattice fringe spacing of PBNC was found to be 0.58 nm, which corresponds to the (002) plane of cellulose (Fig. 2c).[32] The selected area electron diffraction (SAED) pattern of PBNC clearly indicates that it is polycrystalline in nature, which is in accordance with XRD data (Fig. 2d).

The FTIR and XRD analyses of PBNC were performed to study the functional groups and crystallinity of synthesised PBNC nanocellulose.[33] Fig. 3a shows the XRD pattern of PBNC with a major peak at 22° and two minor peaks at 16° and 34°,

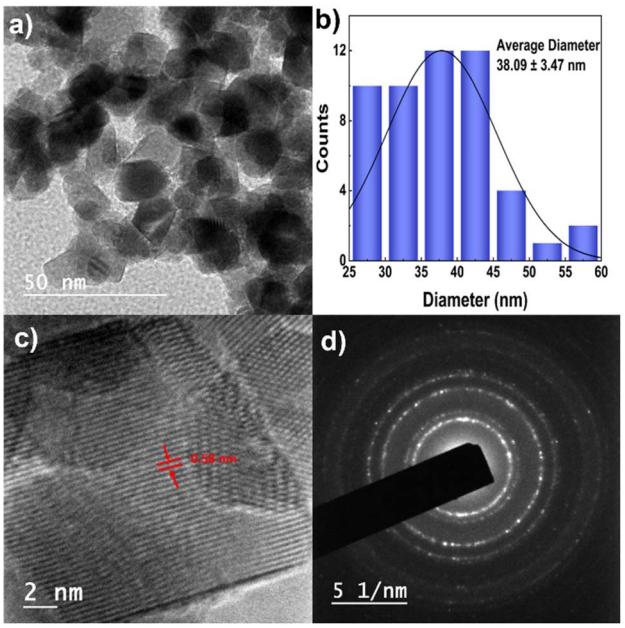

Fig. 2 (a) TEM image of PBNC, (b) size distribution histogram of PBNC, (c) HRTEM image of PBNC, and (d) SAED pattern obtained from PBNC.

corresponding to the (002), (110) and (004) planes, respectively.[34] The investigation of the FTIR spectrum of PBNC is in accordance with the data of previously reported nanocellulose.[35] The bands at or around 1520 cm^{-1} and 1230 cm^{-1} are often assigned to lignin and the peak at 1720 cm^{-1} to lignin and hemicellulose.[36] Upon investigation of the FTIR spectra, we could find the absence of lignin and hemicellulose in PBNC. These findings confirm the synthesis of nanocellulose and also the absence of lignin and hemicellulose contents in the synthesized nanocellulose.[37] Zeta potential studies were carried out on nanocellulose in order to evaluate the surface charge characteristics and colloidal stability. The zeta potential of *Plectranthus barbatus* nanocellulose was found to be −26.7 mV, indicating moderate stability[38] (Fig. S3, SI). The negative surface charge of the suspension minimizes the aggregation of the particles.[39]

The characterisation techniques (FTIR, XRD and HRTEM) were selected to correlate the structural attributes of PBNC with its fluorescence behaviour and with Pb(II) sensing performance. FTIR analysis confirms the presence of abundant oxygen-

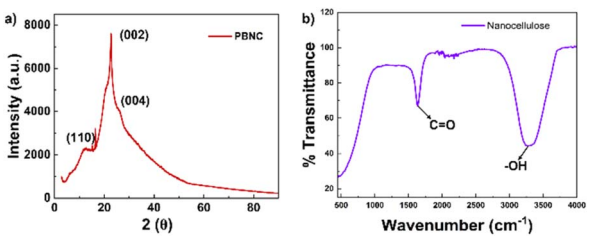

Fig. 3 (a) XRD plot of PBNC with peaks corresponding to the (002), (110) and (004) planes. (b) FTIR spectra of PBNC, with peaks corresponding to carbonyl and hydroxyl groups.

containing functional groups, which serve as active coordination sites for Pb(II) binding, thereby modulating fluorescence intensity.[40] XRD reveals the preservation of cellulose crystallinity following acid hydrolysis, indicating that the ordered crystalline regions contribute to structural stability, which leads to enhanced surface accessibility for metal ion interaction.[41] HRTEM demonstrates the formation of uniformly dispersed nanoparticles with a large specific surface area, facilitating efficient Pb(II) adsorption and fluorescence response.[42] Collectively, these results establish a structure–property relationship, where surface chemistry of nanocellulose governs metal coordination, crystallinity supports optical stability, and nanoscale morphology promotes sensitivity, thereby justifying the relevance of FTIR, XRD, and TEM in elucidating the optical performance of PBNC as a fluorescent probe for Pb(II) ion sensing.

3.3 Optical properties of PBNC and sensing of Pb(II) ions

Cellulose, the precursor of nanocellulose, is generally extracted from plant-based materials by removing lignin, hemicellulose and other organic matter. The luminescence in cellulose-containing materials was attributed to the presence of lignin (a small quantity of lignin residue was presumed to remain even after the synthesis of cellulose) or any other aromatic species generated during the synthesis process.[43] Casten and coworkers presented the theory that the phenylcoumarin and coniferyl structures of lignin are the reason for the fluorescence.[44] This understanding was questioned when Gray and Olmstead suggested, in 1993, that the luminescence in cellulose-based materials was due to the inherent properties of cellulose.[45] The fluorescence of cellulose-based materials prepared from bacterial sources also negates the attribution of luminescence to lignin content, as bacterial sources are free from lignin.[46] Ding *et al.* came up with another explanation for the fluorescence of cellulose-based materials in early 2013.[47] They attributed the fluorescence to the glycosidic bond between glucose molecules present in the structure of cellulose.

The latest theory regarding the intrinsic fluorescence observed in cellulose-based materials is clustering-triggered emission (CTE).[48] The conjugated structures formed by the clustering of oxygen atoms are considered to be the reason for the intrinsic fluorescence of cellulose-based materials. This phenomenon is termed clustering-triggered emission (CTE), and it generally refers to the clustering of electron-rich heteroatoms and/or functional groups. These clusters are formed in a solid state or in an aggregated state, leading to an effective overlap of electron clouds, thus lowering the energy gap and leading to efficient excitation. This clustering increases the conjugation length, leading to the formation of multiple cluster sizes with different energy gaps. The mechanism of clustering triggered emission is still contested. Main molecular interactions that are thought to facilitate the CTE mechanism are (a) overlap of lone pair (nonbonding) orbitals,[49] (b) overlap of lone pair and π orbitals,[50] (c) dipole–dipole interactions[51] and (d) simultaneous rigidification (*via* inter and intramolecular interactions),[52] combined with clustering of delocalized electrons of various functional groups. The clustering of ether, hydroxyl and carbonyl units causes the delocalization of electron density in cellulose-based materials. These phenomena are believed to contribute to the fluorescence in cellulose materials.[53]

The optical properties of PBNC were analysed using UV-Visible spectroscopy and PL spectroscopy. The UV-Visible spectrum indicated two types of electronic transitions occurring in PBNC. The PBNC showed peaks at 228 nm (C=C) and 271 nm (C=O) in the UV-Visible absorption spectrum, corresponding to the transitions π–π^* and n–π^*, respectively (Fig. 4a).[54] These transitions may arise due to the presence of π-conjugated domains or surface defects on PBNC. The absorption tail extending to the longer wavelength may arise from the low-energy transitions of the functional groups present on the surface of PBNC. PBNC showed excitation wavelength-dependent emissions when excited at different wavelengths ranging from 220 to 400 nm (Fig. 4b). The maximum emission (λ_{max}) is observed at 315 nm when PBNC was excited at 220 nm (Fig. 4c). The quantum yield of PBNC was calculated to be 4.43%. The fluorescence lifetime of PBNC was found to be 0.6225 ns after fitting the decay curve with a multi-exponential function (Fig. 4d). This indicates that PBNC has a short and multicomponent lifetime involving non-radiative processes.[55]

3.4 Sensing of Pb(II) ions using PBNC

The PL studies were performed on aqueous solutions of PBNC in the presence of Mn(II), Ba(II), Al(II), Ni(II), Na(I), Pb(II), Fe(II) and Hg(II) metal ions, under the same conditions. The fluorescence analysis revealed that the quenching response of PBNC is selective towards Pb(II) ions (38.9% quenching upon addition of 20 μL of 10^{-5} M Pb(II)) (Fig. 5a). There is no significant difference in the intensities with the other metal ions, which makes PBNC a potential sensor for the selective detection of Pb ions.

The PL studies were conducted for the mixture of PBNC and selected set of metal ions (with and without Pb(II) ions) (Fig. 6a). The fluorescence studies were also conducted for (i) PBNC with various metal ions and Pb(II) ions, and (ii) PBNC with Pb(II) ions alone (Fig. 6b). From both the studies, it was confirmed that the quenching is selectively due to Pb(II) ions. These data further verify specific interaction of PBNC with Pb(II) ions, which is primarily due to the specific binding interactions. From the above studies, PBNC was found to be capable of the selective detection of Pb(II), which makes it a potential candidate for a fluorescent probe.

The PL intensity of PBNC quenched linearly with the increase in the concentration of Pb(II) ions within the range of 0–30 nM. A linear relationship was observed between the concentration of Pb(II) ions and the fluorescence quenching of PBNC. With the increase in the concentration of Pb(II) ions, there occurred a substantial quenching response for PBNC. This linear quenching response of PBNC to Pb ions shows the sensitivity of PBNC towards Pb ions (Fig. 5b).

The fluorescence quenching followed the Stern–Volmer equation,[56] establishing a linear relationship between the relative intensity I/I_o and concentration of Pb(II) with $R^2 = 0.99963$ (Fig. 7a). The detection limit of Pb(II) was calculated to be

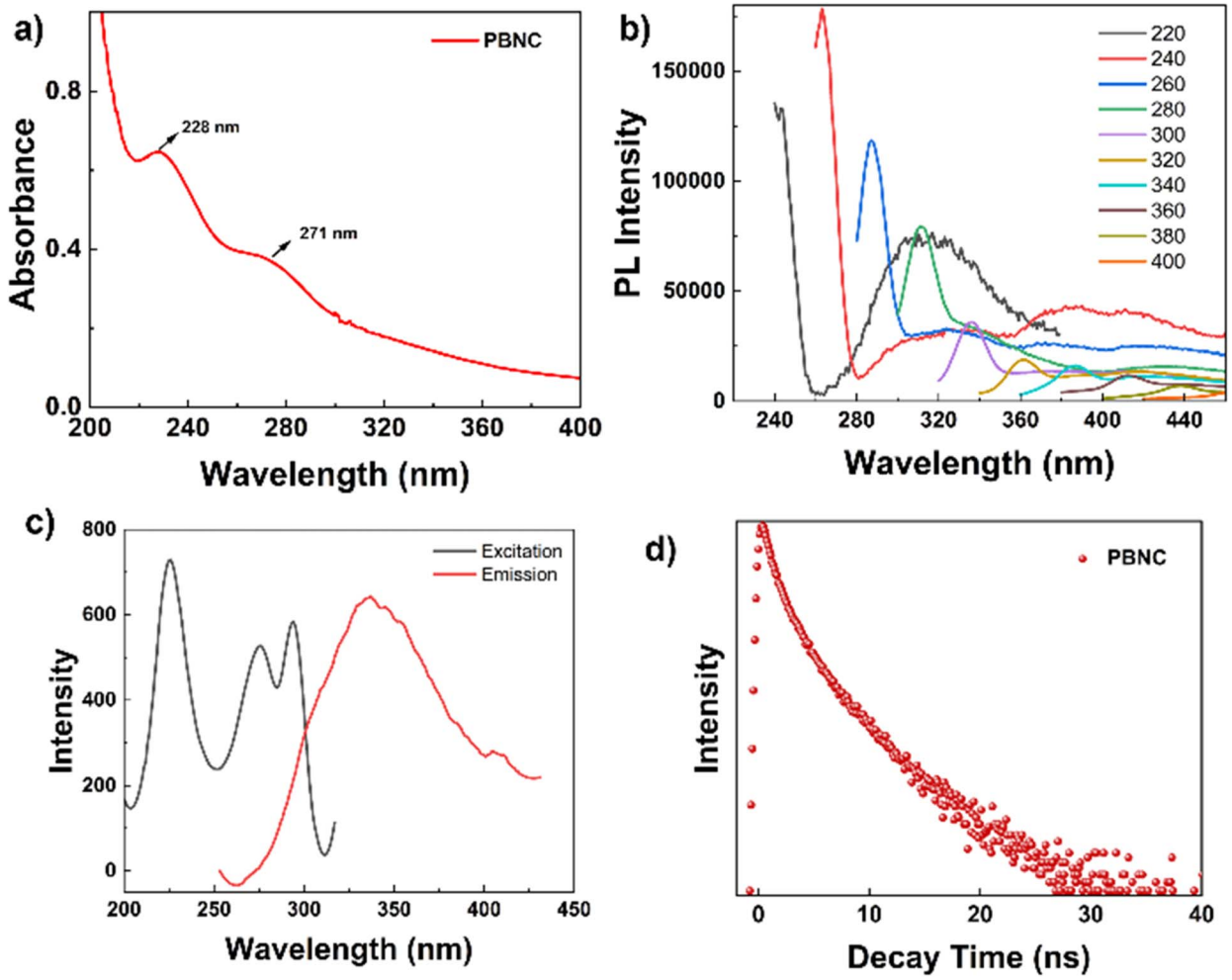

Fig. 4 (a) UV-Visible absorption spectra of *Plectranthus barbatus* nanocellulose, (b) the plot of excitation wavelength-dependent PL emissions of *Plectranthus barbatus* nanocellulose, and (c) excitation spectrum (emission at 315 nm) and the emission spectrum ($\lambda_{ex} = 220$ nm), and (d) plot of fluorescence life time of PBNC.

2.7 nM. Job's plot analysis was used to study the binding of Pb(II) ions with PBNC, by measuring the absorbance across different concentrations of Pb(II) ions.[57]

The stoichiometric ratio between Pb(II) ions and PBNC was determined using the Job's method of continuous variation, wherein a series of solutions were prepared by varying the mole fraction of Pb(II) (10^{-5} M) while maintaining a constant total molar concentration of the two components. The absorbance of each mixture was recorded after equilibrating it for 3 minutes, and the absorbance was plotted against the mole fraction of

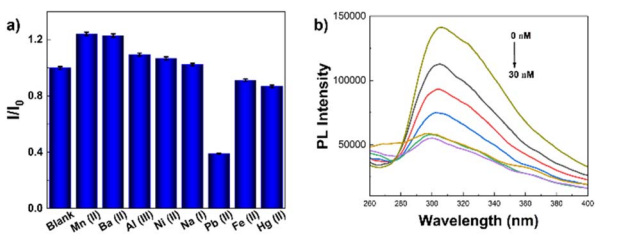

Fig. 5 (a) The PL response of PBNC to various metal ions, and (b) the PL response of PBNC upon sequential addition of Pb(II) ions. I_0 and I are the PL intensities in the absence and presence of metal ions respectively at 315 nm ($\lambda_{ex} = 220$ nm). (Error amount, 3%; *Y* axis error bar of both [±] deviation).

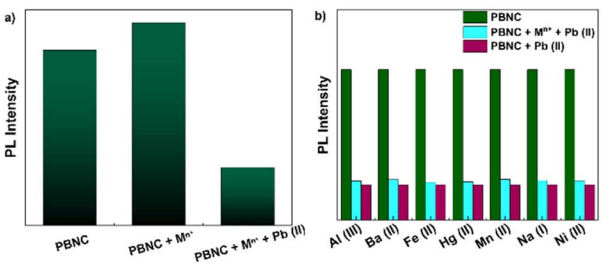

Fig. 6 (a) The PL spectra of PBNC in response to the mixture of metal ions (Al(III), Ba(II), Fe(II), Hg(II), Mn(II), Na(I) and Ni(II)), both in the presence and absence of Pb(II) ions and (b) the PL intensity at 315 nm of PBNC with other metal ions added with Pb(II) ions, and Pb(II) ions alone in PBNC, respectively.

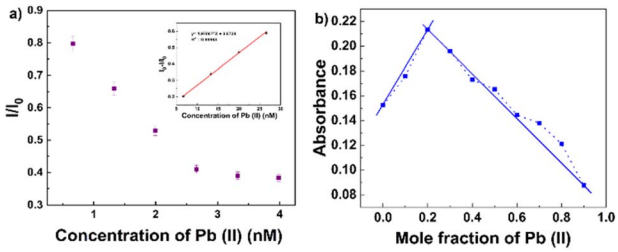

Fig. 7 (a) The plot of I/I_0 against the concentration of Pb(II), and the inset shows the fitted plot at the lower concentrations). (Error amount, 3%; *Y* axis error bar of both [±] deviation). (b) Job's plot was plotted using the mole fraction of Pb(II) ions on the *x*-axis *versus* the absorbance on the *y*-axis.

Pb(II). Using the Job plot, the binding ratio of PBNC to Pb(II) ions was found to be 1 : 0.2 (Fig. 7b).

The commonly proposed mechanisms to explain fluorescence quenching of the probe upon interaction with the analyte include static quenching, dynamic quenching, Förster resonance energy transfer (FRET), and the inner filter effect.[58] Static quenching arises from the formation of a non-fluorescent ground-state complex between the fluorophore and quencher; however, dynamic quenching results from collisional encounters between the excited fluorophore and quencher during its lifetime. Förster resonance energy transfer (FRET) involves a non-radiative energy transfer from the donor fluorophore to an acceptor when their spectral overlap and proximity are favorable. The inner filter effect, originates from the reabsorption or scattering of the excitation or emission light by the quencher.[59] These mechanisms may operate independently or simultaneously, and their contributions need to be assessed to rationalize the quenching behaviour of fluorescent systems. While a comprehensive mechanistic investigation into the fluorescence quenching of PBNC by Pb(II) ions lies beyond the scope of this study, a scientifically grounded and plausible mechanism is nonetheless proposed to support the observed phenomena. In this study, the fluorescence quenching behavior

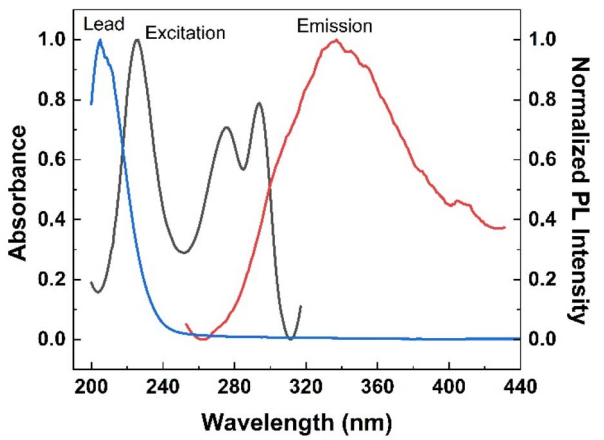

Fig. 8 The UV-Visible absorption spectrum of Pb(II) ions (blue), excitation spectrum of PBNC (emission recorded at 315 nm) (black), and emission spectrum of PBNC (λ_{ex} = 220 nm) (red), respectively.

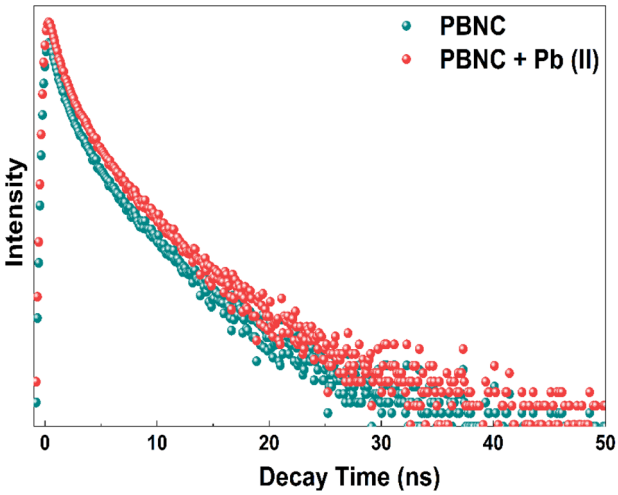

Fig. 9 Fluorescence lifetime of PBNC alone and PBNC in the presence of Pb(II) ions.

of PBNC in the presence of Pb(II) ions is predominantly ascribed to the inner filter effect, which is expected to play a central role in modulating the optical response of the system.[60,61] This occurs due to the spectral overlap between the absorption band of Pb(II) ions and the excitation and/or emission bands of PBNC. As illustrated in Fig. 8, Pb(II) ions exhibit an absorption peak at 205 nm, while PBNC shows excitation and emission peaks at 220 nm and 315 nm, respectively. The pronounced spectral overlap between the absorption band of Pb(II) ions and the excitation band of PBNC strongly substantiates the inner filter effect as a key mechanism responsible for the quenching of photoluminescence intensity upon interaction with Pb(II) ions.

Also, the fluorescence lifetime of PBNC increased from 0.6225 ns to 1.240 ns upon addition of Pb(II) ions, while the PL intensity decreased significantly, as given in Fig. 9. This behaviour rules out dynamic quenching, as dynamic processes reduce both PL intensity and lifetime simultaneously.[62] The observed results indicate static quenching through ground-state complex formation between Pb(II) and oxygen-containing functional groups of PBNC. The formation of non-fluorescent PBNC-Pb(II) complexes reduces the number of emissive centers, leading to a decrease in PL intensity. Simultaneously, coordination of Pb(II) to PBNC modifies surface electronic states and suppresses fast non-radiative pathways, resulting in prolonged excited-state lifetime of the remaining emissive species.[63] Accordingly, the PL quenching of PBNC towards Pb(II) ions is attributed to a combination of static quenching and the inner filter effect.

3.5 Real water sample analysis

PBNC was used for the selective and sensitive detection of Pb ions in a real water sample – lake water. The concentration of Pb ions in the sample was below the detection limit of the proposed method, due to which different concentrations of Pb ions were spiked into the samples and used for fluorescence analysis. The spike recoveries for the quantitative

Table 1 Results of Pb(II) detection in real sample (lake water)

SI. no.	Sample	Added (μM)	Found (μM)	Recovery (%)	RSD (%, $n = 3$)
1	Lake water	10	10.16	101.60	4.33
		20	20.00	100.01	4.56
		30	29.86	99.56	5.27
		40	40.13	100.32	4.53
		50	49.91	99.83	5.23

determination of Pb ions in lake water were performed using PBNC by adding varying concentrations of Pb ions (10, 20, 30, 40, and 50 μM, respectively). The concentrations of Pb ions in the real samples were found (by linear fitting the plot of concentration of Pb ions *versus* the PL intensity (Fig. S4, SI)), and the results are presented in Table 1. The Pb ion detection in real samples ranged from 99.83% to 101.60% at five spiked concentrations. The relative standard deviations (RSDs) varied between 4.33% and 5.27%. This indicates that the sensor has good accuracy and can be used for the detection of Pb(II) ions in real samples.

4 Conclusions

In this work, a novel and efficient autofluorescent nanocellulose, PBNC, was synthesised from the *Plectranthus barbatus* plant, a first of its kind, through an optimized synthesis route. The inherent autofluorescent properties of nanocellulose are used as an analytical signal to develop this optical sensor. PBNC was used to detect toxic Pb(II) ions in aqueous solutions based on the fluorescence quenching mechanism. The quantum yield of PBNC was found to be 4.43%. The novelty of this study lies in utilizing the autofluorescence of PBNC, eliminating the need for incorporating additional sensing agents or fluorescent materials. Previous studies on fluorescence-based metal ion detection have primarily utilized nanocellulose as a supporting substrate rather than using it as an active sensing material.[64] PBNC as an autofluorescent nanocellulose was found to be simple, highly selective and sensitive, cost-effective, and free from the need for chemical modification. The fluorescence intensity of PBNC was quenched by Pb(II) ions, exhibiting a strong linear correlation between the fluorescence response and Pb(II) concentration, with a detection limit of 2.7 nM. These results indicate that PBNC can be employed to design and develop an effective fluorescent probe for metal ion detection without any further modifications. Such a sensor would be of low cost, sustainable, highly sensitive and selective and possess potential for many future innovations. The reported sensor can be upscaled for real-sample analysis and portable sensing formats, including paper-based devices and on-site detection kits for rapid Pb(II) sensing. Integration with smartphone-assisted fluorescence analysis could further enable point-of-care and field-deployable applications. In addition, systematic evaluation in complex environmental and biological matrices, alongside surface engineering for multi-ion recognition, may expand the scope of PBNC toward simultaneous detection of multiple heavy metals. Such developments are expected to advance plant-derived nanocellulose as a versatile, sustainable sensing material for next-generation environmental surveillance, water quality monitoring, and bioanalytical diagnostics.

Author contributions

Joshua Jose: experimentation, investigation, data curation, original draft, writing – review and editing. Aishwarya Joji Mathew: experimentation, investigation, data curation, writing – original draft, writing – review and editing. Elizabeth Gabriel: experimentation and data curation. Ancilin James: experimentation and data curation. Vinod T. P.: conceptualization, validation, resources, visualization, writing – review and editing, funding acquisition, project administration and supervision.

Conflicts of interest

The authors declare that they have no known competing financial interests or personal relationships that could have appeared to influence the work reported in this paper.

Data availability

The data supporting this article have been included as part of the supplementary information (SI). Supplementary information: Fig. S1: XRD plot of the different synthesis stages of PBNC; Fig. S2: FTIR plot of different synthesis stages of PBNC; and Fig. S3: zeta potential graph of PBNC. See DOI: https://doi.org/10.1039/d5na01139f.

Acknowledgements

Joshua Jose and Aishwarya Joji Mathew are grateful to Christ University for the research fellowship. Vinod T. P.is thankful to Centre for Research Projects (CRP), Christ University, for the Seed Money Grant SMSS-2334. The authors are thankful to Vision Group on Science and Technology (VGST), Govt. of Karnataka for K-FIST-L1 grant (GRD No. 1143).

References

1 P. Kumar Gupta, S. Sai Raghunath, D. Venkatesh Prasanna, P. Venkat, V. Shree, C. Chithananthan, S. Choudhary, K. Surender and K. Geetha, in *Cellulose*, IntechOpen, 2019.
2 R. Kamel, N. A. El-Wakil, A. Dufresne and N. A. Elkasabgy, *International Journal of Biological Macromolecules*, 2020, **163**, 1579–1590.
3 H. Sharifi, J. Tashkhourian and B. Hemmateenejad, *Anal. Chim. Acta*, 2020, **1126**, 114–123.
4 F. L. Migliorini, K. B. R. Teodoro and D. S. Correa, *Cellul. Chem. Technol.*, 2020, **54**, 407–413.
5 M. V. Santos, F. E. Maturi, É. Pecoraro, H. S. Barud, L. R. Lima, R. A. S. Ferreira, L. D. Carlos and S. J. L. Ribeiro, *J. Photochem. Photobiol., A*, 2021, **9**, 617328, DOI: 10.3389/fbioe.2021.617328.
6 L. Donaldson, *Molecules*, 2020, **25**, 2393.

7 H. Zhang and B. Z. Tang, *JACS Au*, 2021, **1**, 1805–1814.
8 Z. Wang, H. Zhang, S. Li, D. Lei, B. Z. Tang and R. Ye, *Top. Curr. Chem.*, 2021, **379**, 14.
9 Y. Wang, Z. Zhao and W. Z. Yuan, *ChemPlusChem*, 2020, **85**, 1065–1080.
10 L. Gan, N. Feng, S. Liu, S. Zheng, Z. Li and J. Huang, *Part. Part. Syst. Charact.*, 2019, **36**, 3, DOI: 10.1002/ppsc.201800412.
11 K. B. R. Teodoro, M. J. Silva, R. S. Andre, R. Schneider, M. A. Martins, L. H. C. Mattoso and D. S. Correa, *Carbohydr. Polym.*, 2024, **324**, 121494.
12 K. Kulbat-Warycha, J. Oracz and D. Żyżelewicz, *Molecules*, 2022, **27**, 8986, DOI: 10.3390/molecules27248986.
13 J. Wu, T. Wang, Y. Zhang and W.-P. Pan, *Bioresour. Technol.*, 2019, **291**, 121859.
14 M. F. Cordeiro, T. R. S. Nunes, F. G. Bezerra, P. K. M. Damasco, W. A. V. Silva, M. R. A. Ferreira, O. M. C. Magalhães, L. A. L. Soares, I. M. F. Cavalcanti, M. G. R. Pitta and M. J. B. M. Rêgo, *Braz. J. Microbiol.*, 2022, **82**, e236297, DOI: 10.1590/1519-6984.236297.
15 J. Jose and T. P. Vinod, *New J. Chem.*, 2025, **49**, 9475–9483, DOI: 10.1039/D5NJ01022E.
16 L. U. S. Faria, B. J. S. Pacheco, G. C. Oliveira and J. L. Silva, *J. Mater. Res. Technol.*, 2020, **9**, 12346–12353.
17 W. J. Orts, J. Shey, S. H. Imam, G. M. Glenn, M. E. Guttman and J.-F. Revol, *J. Polym. Environ.*, 2005, **13**, 301–306.
18 B. Zhu, S. Sun, Y. Wang, S. Deng, G. Qian, M. Wang and A. Hu, *J. Mater. Chem. C*, 2013, **1**, 580–586.
19 M. N. Khan, N. Rehman, A. Sharif, E. Ahmed, Z. H. Farooqi and M. I. Din, *International Journal of Biological Macromolecules*, 2020, **153**, 72–78.
20 K. S. Prado and M. A. S. Spinacé, *International Journal of Biological Macromolecules*, 2019, **122**, 410–416.
21 R. Chen, Q. Zhang, Y. Gu, L. Tang, C. Li and Z. Zhang, *Anal. Chim. Acta*, 2015, **853**, 579–587.
22 J. Liang, B. Liu, X. Li, X. Mo, C. Qin, C. Liang, C. Huang and S. Yao, *Bioresour. Technol.*, 2023, **384**, 129328.
23 S. Si, Y. Chen, C. Fan, H. Hu, Y. Li, J. Huang, H. Liao, B. Hao, Q. Li, L. Peng and Y. Tu, *Bioresour. Technol.*, 2015, **183**, 248–254.
24 R. Koshani, J. E. Eiyegbenin, Y. Wang and T. G. M. van de Ven, *J. Colloid Interface Sci.*, 2022, **607**, 134–144.
25 W. Jung, D. Savithri, R. Sharma-Shivappa and P. Kolar, *Energies*, 2018, **11**, 376.
26 Y. Song, J. Zhang, X. Zhang and T. Tan, *Bioresour. Technol.*, 2015, **193**, 164–170.
27 X. Li, Y. Ding, X. Pan, Y. Xing, B. Zhang, X. Liu, Y. Tan, H. Wang and C. Li, *J. Energy Chem.*, 2022, **67**, 492–499.
28 H. Du, M. Parit, K. Liu, M. Zhang, Z. Jiang, T.-S. Huang, X. Zhang and C. Si, *ACS Appl. Mater. Interfaces*, 2021, **13**, 32115–32125.
29 Y. C. Ching and T. S. Ng, *BioResources*, 2014, **9**, 6373–6385.
30 K. Liu, H. Du, T. Zheng, H. Liu, M. Zhang, R. Zhang, H. Li, H. Xie, X. Zhang, M. Ma and C. Si, *Carbohydr. Polym.*, 2021, **259**, 117740, DOI: 10.1016/j.carbpol.2021.117740.
31 Y. Zhu, Z. Wei, F. Jiang, W. Hu, X. Yu and S. Du, *Carbohydr. Polym.*, 2024, **342**, 122419.
32 A. Kumar, S. Asu, P. Mukherjee, P. Singh, A. Kumari and S. K. Sahu, *J. Phys. Chem. Lett.*, 2021, **406**, 113019.
33 Q. Qin, X. Zhang, B. Gao, W. Liu, L. Han, S. L. Sing and X. Liu, *International Journal of Biological Macromolecules*, 2024, **257**, 127944.
34 K. J. Mintz, M. Bartoli, M. Rovere, Y. Zhou, S. D. Hettiarachchi, S. Paudyal, J. Chen, J. B. Domena, P. Y. Liyanage, R. Sampson, D. Khadka, R. R. Pandey, S. Huang, C. C. Chusuei, A. Tagliaferro and R. M. Leblanc, *Carbon*, 2021, **173**, 433–447.
35 H. Du, C. Liu, Y. Zhang, G. Yu, C. Si and B. Li, *Ind. Crops Prod.*, 2016, **94**, 736–745.
36 V. S. Borovkova, Y. N. Malyar, I. G. Sudakova, A. I. Chudina, D. V. Zimonin, A. M. Skripnikov, A. V. Miroshnikova, V. A. Ionin, A. S. Kazachenko, V. V. Sychev, I. S. Ponomarev and N. Issaoui, *Polymers*, 2022, **14**, 4521.
37 A. Barhoum, J. Jeevanandam, A. Rastogi, P. Samyn, Y. Boluk, A. Dufresne, M. K. Danquah and M. Bechelany, *Nanoscale*, 2020, **12**, 22845–22890.
38 W. Huo, X. Zhang, K. Gan, Y. Chen, J. Xu and J. Yang, *J. Eur. Ceram. Soc.*, 2019, **39**, 574–583.
39 R. R. Retamal Marín, F. Babick and L. Hillemann, *Colloids Surf., A*, 2017, **532**, 516–521.
40 H. Xu, M. Yan, W. Li, H. Jiang and L. Guo, *Water Res.*, 2018, **144**, 435–443.
41 A. Grząbka-Zasadzińska, I. Ratajczak, K. Król, M. Woźniak and S. Borysiak, *Cellulose*, 2021, **28**, 5745–5759.
42 A. Abdullah, A. N. Kursunlu and E. Guler, *RSC Adv.*, 2023, **13**, 2683–2691.
43 J. Poisson and K. Zhang, *Acc. Mater. Res.*, 2024, **5**, 920–932.
44 B. Albinsson, S. Li, K. Lundquist and R. Stomberg, *J. Mol. Struct.*, 1999, **508**, 19–27.
45 J. A. Olmstead and D. G. Gray, *J. Phys. Chem. Lett.*, 1993, **73**, 59–65.
46 R. Stephen Davidson, L. A. Dunn, A. Castellan and A. Nourmamode, *J. Photochem. Photobiol., A*, 1991, **58**, 349–359.
47 Q. Ding, W. Han, X. Li, Y. Jiang and C. Zhao, *Sci. Rep.*, 2020, **10**, 21387.
48 Y. Gong, Y. Tan, J. Mei, Y. Zhang, W. Yuan, Y. Zhang, J. Sun and B. Z. Tang, *Sci. China:Chem.*, 2013, **56**, 1178–1182.
49 J. Wang, L. Xu, S. Zhong, Y. Yang, G. Feng, Q. Meng, Y. Gao and X. Cui, *Polym. Chem.*, 2021, **12**, 7048–7055.
50 P. Liao, J. Huang, Y. Yan and B. Z. Tang, *Mater. Chem. Front.*, 2021, **5**, 6693–6717.
51 W. Xu, D. Hu, Z. Wang, G. Wang, K. Liu, J. Liang, R. Miao and Y. Fang, *J. Phys. Chem. Lett.*, 2022, **13**, 5358–5364.
52 Q. Zhou, B. Cao, C. Zhu, S. Xu, Y. Gong, W. Z. Yuan and Y. Zhang, *Small*, 2016, **12**, 6586–6592.
53 S. Tang, T. Yang, Z. Zhao, T. Zhu, Q. Zhang, W. Hou and W. Z. Yuan, *Chem. Soc. Rev.*, 2021, **50**, 12616–12655.
54 J. Kim, H. J. Shim, J. Yang, M. K. Choi, D. C. Kim, J. Kim, T. Hyeon and D. Kim, *Adv. Mater.*, 2017, **29**, 38, DOI: 10.1002/adma.201700217.
55 Z. Zhang, G. Liu, X. Li, S. Zhang, X. Lü and Y. Wang, *ChemPlusChem*, 2020, **85**, 487–502.

56 X. Zhou, X. Gao, M. Liu, C. Wang and F. Chu, *Microchim. Acta*, 2017, **184**, 4175–4181.
57 S. Shanmuga Priya and S. Suseem, *RSC Adv.*, 2024, **14**, 17471–17479.
58 F. Zu, F. Yan, Z. Bai, J. Xu, Y. Wang, Y. Huang and X. Zhou, *Microchim. Acta*, 2017, **184**, 1899–1914.
59 L. Pei, W. Zhang, S. Yang, K. Chen, X. Zhu, Y. Zhao and S. Han, *J. Fluoresc.*, 2023, **33**, 1147–1156.
60 M. Zheng, Z. Xie, D. Qu, D. Li, P. Du, X. Jing and Z. Sun, *ACS Appl. Mater. Interfaces*, 2013, **5**, 13242–13247.
61 A. J. Mathew, T. P. Vinod and Y. Nair, *Nanoscale Adv.*, 2025, **7**, 7836–7845, DOI: 10.1039/D5NA00892A.
62 G. Hollett, D. S. Roberts, M. Sewell, E. Wensley, J. Wagner, W. Murray, A. Krotz, B. Toth, V. Vijayakumar and M. J. Sailor, *J. Phys. Chem. C*, 2019, **123**, 17976–17986.
63 D. Genovese, M. Cingolani, E. Rampazzo, L. Prodi and N. Zaccheroni, *Chem. Soc. Rev.*, 2021, **50**, 8414–8427.
64 T. Park, N. Kim, D. Kim, S.-W. Kim, Y. Oh, J.-K. Yoo, J. You and M.-K. Um, *ACS Appl. Mater. Interfaces*, 2019, **11**, 48239–48248.